Title

A deep intronic variant in *MME* causes autosomal recessive Charcot-Marie-Tooth neuropathy through aberrant splicing.

Authors

Bianca R Grosz[1,2], Jevin M Parmar[3,4], Melina Ellis[1,2], Samantha Bryen[5,6], Cas Simons [5,6], Andre L.M. Reis[5,7,8], Igor Stevanovski[5,7], Ira W. Deveson[5,7,8], Garth Nicholson[2,11], Nigel Laing[3], Mathew Wallis[9,10], Gianina Ravenscroft[3], Kishore R. Kumar[2,11,12,13], Steve Vucic[2,14], Marina L Kennerson[1,2,11]

ORCID:

Bianca R Grosz: 0000-0002-6926-0551

Jevin Parmar: 0000-0003-1864-8094

Melina Ellis: 0000-0002-8542-048X

Samantha Bryen: 0000-0002-4140-8622

Cas Simons: 0000-0003-3147-8042

Andre L.M Reis: 0000-0002-7300-1157

Igor Stevanovski: 0000-0002-7713-1979

Ira W Deveson: 0000-0003-3861-0472

Mathew Wallis: 0000-0002-5441-1732

Garth A Nicholson: 0000-0001-9694-066X

Nigel Laing: 0000-0001-5111-3732

Gianina Ravenscroft: 0000-0003-3634-211X

Kishore R Kumar: 0000-0003-3482-6962

Marina L Kennerson: 0000-0003-3332-5074

Affiliations:

1. Northcott Neuroscience Laboratory, ANZAC Research Institute, Sydney, NSW 2139, Australia
2. The University of Sydney, Camperdown, NSW, 2050, Australia
3. Rare Disease Genetics and Functional Genomics Research Group, Harry Perkins Institute of Medical Research, QEII Medical Centre, Nedlands, Western Australia, 6009, Australia
4. Centre for Medical Research, Faculty of Health and Medical Sciences, The University of Western Australia, Perth, WA 6009, Australia
5. Centre for Population Genomics, Garvan Institute of Medical Research, and UNSW Sydney, Sydney, NSW, Australia
6. Centre for Population Genomics, Murdoch Children's Research Institute, Melbourne, VIC, Australia
7. Genomics and Inherited Disease Program, Garvan Institute of Medical Research, Sydney, NSW, Australia.
8. Faculty of Medicine, University of New South Wales, Sydney, NSW, Australia.
9. Tasmanian Clinical Genetics Service, Tasmanian Health Service, Hobart, TAS, Australia.
10. School of Medicine and Menzies Institute for Medical Research, University of Tasmania, Hobart, TAS, Australia.
11. Molecular Medicine Laboratory and Neurology Department, Concord Repatriation General Hospital, Hospital Rd, Concord, NSW, 2139, Australia
12. Translational Neurogenomics Group, Genomic and Inherited Disease Program, The Garvan Institute of Medical Research, 384 Victoria St, Darlinghurst, NSW, 2010, Australia
13. St Vincent's Healthcare Campus, Faculty of Medicine, UNSW Sydney, Level 5, De Lacy Building, St Vincent's Hospital, Darlinghurst, NSW, 2010, Australia.
14. Brain and Nerve Research Centre, The University of Sydney, Sydney, NSW 2139, Australia

Abstract

Background: Loss-of-function variants in *MME* (membrane metalloendopeptidase) are a known cause of recessive Charcot-Marie-Tooth Neuropathy (CMT). A deep intronic variant, *MME* c.1188+428A>G (NM_000902.5), was identified through whole genome sequencing (WGS) of two Australian families with recessive inheritance of axonal CMT using the seqr platform. *MME* c.1188+428A>G was detected in a homozygous state in Family 1, and in a compound heterozygous state with a known pathogenic *MME* variant (c.467del; p.Pro156Leufs*14) in Family 2.

Aims: We aimed to determine the pathogenicity of the *MME* c.1188+428A>G variant through segregation and splicing analysis.

Methods: The splicing impact of the deep intronic *MME* variant c.1188+428A>G was assessed using an *in vitro* exon-trapping assay.

Results: The exon-trapping assay demonstrated that the *MME* c.1188+428A>G variant created a novel splice donor site resulting in the inclusion of an 83 bp pseudoexon between *MME* exons 12 and 13. The incorporation of the pseudoexon into *MME* transcript is predicted to lead to a coding frameshift and premature termination codon (PTC) in *MME* exon 14 (p.Ala397ProfsTer47). This PTC is likely to result in nonsense mediated decay (NMD) of *MME* transcript leading to a pathogenic loss-of-function.

Interpretation: To our knowledge, this is the first report of a pathogenic deep intronic *MME* variant causing CMT. This is of significance as deep intronic variants are missed using whole exome sequencing screening methods. Individuals with CMT should be reassessed for deep intronic variants, with splicing impacts being considered in relation to the potential pathogenicity of variants.

Key Words (up to 5): Charcot-Marie-Tooth disease, splicing, *MME*, recessive, deep intronic

Introduction

Charcot-Marie-Tooth neuropathy (CMT) is the most common inherited peripheral neuropathy, affecting 1/2500 individuals[1]. CMT is characterized by progressive length-dependent loss of peripheral motor and sensory nerves, resulting in distal muscle weakness and sensory symptoms[2]. Patients are broadly divided into subtypes based on whether nerve conduction studies (NCS) indicating demyelinating (CMT1) or axonal (CMT2) forms of the disease. Recessive loss-of-function variants in the membrane metalloendopeptidase (*MME*) gene have been previously reported to cause axonal Charcot-Marie-Tooth neuropathy type 2T (CMT2T; OMIM: #617017)[3–11]. *MME* encodes for neprilysin, a widely expressed membrane-bound metallopeptidase that has a key role in neuropeptide processing[12]. A significant portion of patients with axonal CMT remain genetically undiagnosed[13–17], indicating that further disease-causing genes and pathogenic variants in known genes are yet to be identified.

Splicing variants are increasingly being recognized as a cause of Mendelian disease[18,19]. The precise removal of introns (non-coding regions) and inclusion of exons (coding regions) in the final mature mRNA relies on the spliceosome and auxiliary splicing factors recognizing specific sequence motifs, such as the 5' donor splice site and 3' acceptor splice site. Splice-altering variants can weaken or abolish recognition of the correct splice sites, or alternatively strengthen or create cryptic splice sites that mimic consensus splicing sequences[20]. These variants typically lead to one or more mis-splicing events that result in the skipping of partial or complete exons, and/or the retention of partial or complete introns [21–42]. Pathogenic splicing variants have been found in several CMT genes including *MPZ*[21,30,39,40], *MFN2*[22,30,31], *LRSAM1*[23], *IGHMBP2*[24], *INF2*[25], *MCM3AP*[26], *SH3TC2*[30,32,38], *GDAP1*[27,42], *SBF1*[28], *NDRG1*[37], and *FGD4*[29]. Variants affecting canonical splice donor and acceptor sites have also been described in *MME* [4,41].

Exon-trapping, also known as a mini-gene assay, is an *in vitro* technique used to identify exons in a genomic region of interest[43]. This is of particular use when relevant patient tissue is unavailable or when relevant transcripts may be unstable or degraded by nonsense mediated decay (NMD) [44]. The genomic region of interest is cloned into an exon-trapping vector between two known exons. This exon-trapping vector is transfected into a cell line where it is transcribed and undergoes a series of post-transcriptional processes that include pre-mRNA splicing to create mature mRNA. This mRNA consists of the 'trapped' exons of the genomic region of interest flanked by the known exons, which can then be Sanger sequenced to characterize the 'trapped' exons. Comparison of 'trapped' exons between wild type and variant genomic sequences can also indicate if a candidate variant affects splicing [45–51]. The well-validated exon-trapping vector pSpliceExpress [52] consists of known exons of the rat insulin gene, *Ins2*, and has been used previously to determine the splicing impacts of multiple pathogenic variants in Mendelian disease [45–51].

Here we report a deep intronic variant in *MME* [chr3:155142758A>G (hg38); *MME* c.1188+428A>G], found in a recessive state in two Australian families. Exon-trapping revealed that this variant creates a novel splice donor site in *MME* intron 12 (NM_000902.5) which, along with a preceding existing cryptic splice acceptor site, results in the incorporation of an 83 bp pseudoexon in the *MME* transcript [chr3:155,142,675-155,142,757 (hg38); r.1188_1189ins[1188+345_1188+427]]. The coding frameshift caused by this pseudoexon leads to a PTC in exon 14 and likely NMD of the *MME* transcript (p.Ala397ProfsTer47), resulting in a loss of *MME* function.

Materials and Methods:

Subjects

Members of Family 1 were recruited and informed consent was obtained for this study using protocols approved by the Sydney Local Health District Human Ethics Research Committee (2019/ETH07839). Recruitment and informed consent for the proband of Family 2 was approved by the Human Research Ethics Committee of the Royal Melbourne Hospital (HREC/16/MH/251).

Variant Detection

Genomic DNA for Family 1 was extracted from peripheral blood using the PureGene Kit (Qiagen) following the manufacturer's instructions. WGS for two individuals in Family 1 (V:1 and V:3) was outsourced to the Garvan Sequencing Platform. Paired-end sequencing reads of 150 base pairs were generated using the Illumina NovaSeq 6000 sequencing machine, with 30-fold average read depth.

In Family 2, genomic DNA for the proband was extracted at the Department of Diagnostic Genomics (PathWest, Perth, Australia) using the QIAsymphony^{SP} machine and QIAsymphone® DSP DNA Midi Kit. The proband underwent WGS at the Australian Genomics Research Facility (AGRF), Melbourne, following GATK4 best-practices. Paired-end sequencing reads of 150 base pairs were generated using the Illumina NovaSeq 6000 sequencing machine, with 30-fold average read depth. Parental DNA was not available for sequencing.

WGS data processing was performed at the Centre for Population Genomics (CPG) following the DRAGEN GATK best practices pipeline. Reads were aligned to the hg38 reference genome using Dragmap (v1.3.0). Cohort-wide joint calling of single nucleotide variants (SNVs) and small insertion/deletion (indel) variants was performed using GATK

HaplotypeCaller (v4.2.6.1) with "--dragen-mode" enabled. Sample sex and relatedness quality checks were performed using Somalier (v0.2.15)[53]. Variants were annotated using VEP 105, and loaded into the web-based variant filtration platform, seqr[54]. A WGS search was conducted using the seqr[45] platform for low minor allele frequency (<0.01) variants in CMT-related genes, for both Family 1 and 2 [gene list- Hereditary Neuropathy_CMT_IsolatedAndComplex (Version 2.14)[55]]. Additionally, variants were analyzed by the CPG Automated Interpretation Pipeline (AIP, https://github.com/populationgenomics/automated-interpretation-pipeline). *In silico* splicing analysis was conducted using SpliceAI [56].

Segregation Analysis

The *MME* c.1188+428A>G variant in Family 1 and Family 2 was amplified using primers that spanned *MME* intron 12 (5'-CTCAGCCGAACCTACAAGGA-3'; 5'-GCAAATGCTGCTTCCACAT-3') to produce a 1264 bp amplicon [chr3:155,142,289-155,143,552 (hg38)]. An internal sequencing primer was used (5'-CTGTGTTAAAAGTAATTTCGGGG-3') and the amplicon was Sanger sequenced. The *MME* c.467del variant in Family 2 was amplified (5'-GCAGAGCCGTATGCATCACT-3'; 5'-TTCAGCTGTCCAAGAAGCACC-3'). A 717bp amplicon was produced [chr3:155,116,171-155,116,887 (hg38)], which was subsequently Sanger sequenced.

Sanger Sequencing

For Family 1, PCR amplicons were sent to Garvan Molecular Genetics, Garvan Institute (Sydney, Australia) for Sanger sequencing using BigDye Terminator cycle sequencing protocols. For Family 2, proband PCR amplicons were Sanger sequenced at AGRF, Perth using BigDye Terminator sequencing protocols. Sequences were visualized and analyzed using Snapgene Software version 7.1 (www.snapgene.com).

Oxford Nanopore Technologies (ONT) Long Read Sequencing

High molecular weight (HMW) DNA samples of the Proband in Family 2 were transferred to the Garvan Sequencing Platform for targeted long-read sequencing analysis on ONT instruments. Prior to ONT library preparations, DNA was sheared to ~20-25 kb fragment size using a MegaRuptor 3 instrument and visualized post-shearing on an Agilent FemtoPulse.

Sequencing libraries were prepared from ~3-5 µg of HMW DNA, using native library prep kit SQK-LSK114, according to manufacturer's instructions. Each library was loaded onto a R10.4.1 flow cell and sequenced on a PromethION device with live target selection/rejection executed by the ReadFish software package[57]. Detailed descriptions of software and hardware configurations used for ReadFish are provided in a previous publication[58]. Samples were run for a maximum duration of 72 h, with nuclease flushes and library reloading performed at approximately 24- and 48-h timepoints for targeted sequencing runs, to maximize sequencing yield. Raw ONT sequencing data was converted to BLOW5 format[59] using slow5tools (v.0.3.0)[60] then base-called using Guppy (v6). Resulting FASTQ files were aligned to the hg38 reference genome using minimap2 (v2.14-r883)[61]. Variants were called using clair3[62], phased using Whatshap[63] and visualized using the Integrative Genomics Viewer (IGV, v2.17.3)[64].

Cell Culture

The human HeLa cervical epithelial cell line (ATCC) was maintained in Dulbecco's Modified Eagle's Medium (DMEM)(Gibco) containing 10% (v/v) fetal bovine serum (FBS) (Gibco), +100 U/mL penicillin (Gibco), and 100 µg/mL streptomycin (Gibco) at 37°C in humidified air and 5% CO2.

Cloning Procedures

The region surrounding *MME* c.1188+428A>G [chr3:155,141,790-155,143,755 (hg38)] was amplified from the genomic DNA of a heterozygous carrier of the c.1188+428A>G variant, using *attB* adapter primers (5'-AAAAAGCAGGCTTCGCTCTTAAATGGTTGGCTT-3'; 5'-AGAAAGCTGGGTAACTAGACTCTTGGGGAAGGC -3'). The *MME* amplicon was then cloned into the exon-trapping pSpliceExpress vector between flanking *Ins2* exons using a two-step Gateway cloning BP reaction (ThermoFisher). pSpliceExpress was a gift from Stefan Stamm (Addgene plasmid #32485)[52]. The pSpliceExpress-*MME* clones were then Sanger sequenced to verify the correct insertion of *MME* and to determine the c.1188+428A>G genotype of each clone (as the genomic DNA template was heterozygous for the variant).

In vitro exon-trapping

HeLa cells were grown to approximately 70% confluence in a 6-well plate. HeLa cells were separately transfected with either 2 µg of pSpliceExpress-MME_{WT} or 2 µg of pSpliceExpress-$MME_{c.1188+428A>G}$ using Lipofectamine 3000 (ThermoFisher). RNA extraction was performed 48 h following transfection using the RNEasy Mini Kit (Qiagen), and reverse-transcribed template was prepared using the iScript cDNA Synthesis Kit (Bio-Rad). PCR amplification of cDNA was conducted using primers designed to anneal to the flanking *Ins2* exons (5'-CAGCACCTTTGTGGTTCTCA-3'; 5'-CAGTGCCAAGGTCTGAAGGT-3'). The RT-PCR amplicons were size fractionated using a 1.5% w/v agarose gel. The largest amplicon for each vector was gel-purified using Isolate II PCR and Gel Kit (Bioline) for Sanger Sequencing.

In silico splicing analysis of reported *MME* variants

All reported *MME* variants in gnomAD v.4.0.0 were detected by searching the gnomAD browser for the genomic region corresponding with the *MME* gene; '3-155024124-155183704'(hg38). The *MME* variants reported in gnomAD were then exported using the

224 'Export Variants to CSV' function. The consequences of the variants were described by
225 gnomAD using the Variant Effect Predictor (VEP) annotation based on the most deleterious
226 predicted functional effect of each variant [65] . These variants were then filtered for a minor
227 allele frequency (MAF) <0.01 and a maximum SpliceAI Δscore >0.8 (high precision splicing
228 change prediction[66]) as annotated by gnomAD.

229

230

231

Results:

Clinical Phenotypes

Family 1 consists of four affected siblings from a consanguineous family of European (non-Finnish) background (Figure 1a). The phenotype was consistent with a generalized sensorimotor axonal neuropathy and sensory ataxia without cerebellar signs (Table 1), and was confirmed with NCS for individuals V:1 and V:6 (Table 2). Affected individuals had previously undergone diagnostic and research whole exome sequencing with negative results.

Family 2 consists of one affected female born to a healthy, non-consanguineous couple (Figure 1b). Neurological examination revealed mild distal upper limb weakness and moderate distal lower limb weakness (Table 1). NCS showed evidence of an axonal sensorimotor neuropathy (Table 2). Bilateral MRI of the thighs and calves showed muscle atrophy (Supplementary Figure 1).

Genetic Analysis

WGS screening using the seqr platform in Family 1 revealed a single homozygous variant in two affected individuals (V:1 and V:3), *MME* c.1188+428A>G (NM_000902.5). This variant was reported in dbSNP build 155[67] (rs61758195), with a low MAF in gnomAD v4.0.0[68] (10/152120), All of Us (35/490,748)[69], and TOPMED[70] (15/264290). No homozygous individuals were reported in gnomAD, All of Us, or TOPMED. SpliceAI predicted that *MME* c.1188+428A>G could create a strong novel splice donor site (Score 0.97; where a SpliceAI score above 0.8 is considered a 'high precision' predicted splice variant[56]). This in turn strengthened the SpliceAI prediction for a cryptic splice acceptor site 83 bp upstream of the novel splice donor site (Score 0.99).

Segregation analysis in Family 1 confirmed the biallelic inheritance of the *MME* c.1188+428A>G variant segregated with the CMT phenotype (Figure 1a). Sanger sequencing of DNA from available individuals showed that all affected individuals were homozygous for the *MME* c.1188+428A>G variant and unaffected individuals were carriers (Supplementary Figure 2).

WGS screening using the seqr platform and AIP was conducted in the proband of Family 2 (II:1). The *MME* c.1188+428A>G variant was detected in a compound heterozygous state with a second *MME* variant (*MME* c.467del; p.Pro156Leufs*14), which has previously been reported as pathogenic[41] (Figure 1b). Sanger sequencing validated the presence of each *MME* variant in the index individual (Supplementary Figure 3). As parental DNA was unavailable, ONT long-read sequencing was conducted to phase the heterozygous *MME* variants in the proband (Figure 1c-d). ONT long-read sequencing confirmed that *MME* c.1188+428A>G (boxed red in Figure 1c) and c.467del (boxed red in Figure 1d) were present on alternative haplotypes (hap-1: red, hap-2: blue) and therefore were in *trans* in the proband.

In vitro exon-trapping of *MME*-pSpliceExpress vectors

Two separate exon-trapping pSpliceExpress vectors were generated to assess the *in vitro* splicing impact of the *MME* c.1188+428A>G variant: pSpliceExpress-MME_{WT} (wild-type) and pSpliceExpress-$MME_{c.1188+428A>G}$ (variant). A schematic of the constructs and relevant SpliceAI scores are shown in Figure 2a. RT-PCR products produced following transfection of these vectors were analyzed using gel electrophoresis (Figure 2b), which revealed a visible size difference between the wild-type (381 bp) and *MME* c.1188+428A>G amplicons (464 bp). The gel-purified amplicons were Sanger sequenced and the sequencing was aligned to the WT *MME* mRNA sequence. The sequenced products showed that the pSpliceExpress-MME_{WT} produced a transcript that was correctly spliced between *MME* exon 12 and 13 (Figure 2c). In contrast, exon-trapping of the pSpliceExpress-$MME_{c.1188+428A>G}$ vector showed that an 83 bp pseudoexon had been spliced between *MME* exon 12 and 13 (Figure 2d). A BLAT search[71] using the sequence of the trapped pseudoexon revealed alignment to the intronic region directly upstream of the *MME* c.1188+428A>G variant [chr3:155,142,675-155,142,757 (hg38)]. This suggests that the *MME* c.1188+428A>G variant creates a novel splice donor site leading to the aberrant inclusion of 83 bp of intronic *MME* sequence in the final spliced transcript, as predicted by SpliceAI. Prediction of the novel *MME* coding sequence caused by the introduction of the pseudoexon showed that a PTC was generated in exon 14 (p.Ala397ProfsTer47) at genomic position chr3:155,144,368 (hg38)(Supplementary Figure 4). This PTC likely leads to NMD of the *MME* transcript.

In silico splicing analysis of *MME* variants

All reported *MME* variants in gnomAD v.4.0.0 were assessed using the integrated SpliceAI scores to determine if splicing variants in *MME* were a likely underrecognized cause of disease. There were 37,264 total variants reported in *MME* in gnomAD, of which 35,673 variants had a MAF <0.01. Of these, 88 variants had a maximum SpliceAI Δscore above 0.8

(Supplementary Table 1). There were no homozygotes reported for any of the 88 *MME* putative splicing variants. The majority of these predicted splicing variants were predicted to directly change either the canonical splice donor sites (26/88) or canonical splice acceptor sites (30/88) of *MME*, including an inframe deletion (c.1317_1317+2del) and a frameshift variant (c.957+1del). An additional nine variants were predicted to affect a splicing region, including one which is also annotated as a synonymous variant (c.1188G>A; p.Lys396Lys). Nine missense variants (p.Asp209Gly, p.Ile217Ser, p.Glu282Val, p.Arg365Ile, p.Ser436Gly, p.Asp533Gly, p.Ile553Val, p.Val554Phe, p.Gln692Arg) and a synonymous variant (p.Gly417Gly) were also predicted to alter splicing. Twelve variants were annotated as 'intron variants', of which two could be considered 'deep intronic' variants (c.1188+428A>G, described in this manuscript, and c.197-9871A>G). Interestingly, further analysis using SpliceAI demonstrated that *MME* c.197-9871A>G was predicted to create a splice donor site (Score 0.81) and strengthen an upstream cryptic splice acceptor site (Score 0.81) in a similar manner to c.1188+428A>G, thereby possibly creating an in-frame 96 bp pseudoexon.

Discussion

Here we report a deep intronic variant, *MME* c.1188+428A>G causing recessive CMT2T in two unrelated Australian families. This variant results in a pseudoexon that likely leads to NMD of the *MME* transcript, resulting in a loss-of-function. This is in keeping with previously reported *MME* variants which have broadly been characterised as 'loss-of-function' variants. To our knowledge, this is the first report of a pathogenic deep intronic variant in *MME*. Given that a significant portion of patients with axonal CMT remain genetically undiagnosed[13–17], it's possible that deep intronic variants in *MME* explain a portion of this diagnostic gap.

Individuals from Family 1 previously underwent both diagnostic WES and research WES, and the proband in Family 2 previously underwent targeted gene panel testing (PathWest neuro v3). These testing methods did not capture deep intronic regions and returned negative results. However, deep intronic regions have previously been shown to have a higher prevalence of variants than coding regions and canonical splice sites[72]. Our findings suggest that intronic SNPs should be analyzed to determine if they impact splicing before they are dismissed as benign. Detection and functional validation of deep intronic variants has previously been shown to increase diagnostic rates in other Mendelian diseases including X-linked Alport syndrome[73], inherited retinal disorders[74,75], and dystrophinopathy[76,77]. Pathogenic deep intronic variants, such as described here, are likely to be underreported amongst CMT-causing genes due to a lack of detection by WES and targeted gene panels, and a lack of functional investigation upon detection.

The *MME* c.1188+428A>G variant was reported in multiple different genetic ancestry groups in gnomAD v.4.0.0[68], including in the European (Non-Finnish) (8/68008), African/African

American (1/41432), and 'remaining' (1/2092) ancestry groups. This was also reflected in the 'All of Us' Research Program[69], which reported the *MME* c.1188+428A>G variant in the African (2/107,888) and European populations (33/256,804). Whilst it is possible that *MME* c.1188+428A>G represents a recurrent *de novo* variant, it is also likely that this variant has persisted at low levels in the global population. As this variant is missed by WES and may not be prioritised by variant-filtering approaches focusing on coding variants, this variant may therefore represent an underappreciated cause of recessive CMT. This is further supported by its detection in two Australian CMT families who are not known to be related.

Whilst the predicted splicing variants reported in *MME* are individually rare, we have described eighty-eight variants in gnomAD that are predicted by SpliceAI to alter splicing. Nine of these variants were annotated as missense variants, and one was a synonymous change. This is of note as these 'missense' variants are often assumed to result in a single amino acid change, and synonymous variants are often considered functionally neutral, with their effect on splicing typically not assessed[78]. Our results suggest that the discovery of any of these eighty-eight variants in a homozygous or compound heterozygous state in an individual with CMT should prompt further functional investigation of their effect on splicing of the *MME* transcript.

Prior to functional validation, *MME* c.1188+428A>G was considered a variant of uncertain significance (VUS) according to American College of Medical Genetics and Genomics (ACMG) criteria[79] (BP4, PM2, PM3, PP1), However, the functional evidence generated by the splicing assay now allows for the addition of PVS1 (null variant in a gene where loss-of-function is a known mechanism of disease) and PS3 (well-established *in vitro* or *in vivo* functional studies supportive of a damaging effect on the gene or gene product) criteria. This allows reclassification of the variant as 'pathogenic'. Therefore, this work demonstrates the

357 importance of functional validation to confirm the effect of candidate variants on splicing to
358 increase diagnostic rates for those with inherited disease.

359 Previously described homozygous *MME* patients typically have a phenotype consistent with
360 late-onset axonal neuropathy. In contrast, three of the four affected siblings in Family 1
361 described childhood onset and the proband of Family 2 described symptom onset in early
362 adulthood. It has also previously been reported that heterozygous *MME* variants can cause
363 spinocerebellar ataxia type 43 (SCA43)[80] as well as autosomal dominant CMT[3]. However,
364 the individuals in Family 1 who were *MME* c.1188+428A>G heterozygotes were all
365 clinically assessed as neurologically normal, including an individual who is in their seventh
366 decade. Homozygous affected individuals in Family 1 were noted to have a sensory ataxia
367 rather than cerebellar ataxia, although MRI brain studies were not conducted. Therefore, our
368 findings here do not support a role for *MME* c.1188+428A>G to cause SCA43 or autosomal
369 dominant CMT, and further expand the phenotype of recessive CMT2T.

370 Understanding the specific effects of splice-affecting variants is crucial for developing
371 potential therapeutic strategies. Antisense oligonucleotides (ASOs) that modulate splicing are
372 an active area of research, including individualized approaches to treat rare genetic
373 diseases[81–83]. Several antisense nucleotides that modify splicing have been approved by the
374 United States Food and Drug Administration and have resulted in marked improvements in
375 clinical outcomes in those with genetic diseases[84–94]. An FDA-approved "n-of-1" ASO,
376 milasen, successfully blocked pathogenic pseudoexon inclusion in *MFSD8* in a patient with
377 neuronal ceroid lipofuscinosis type 7[94]. ASOs which block pathogenic pseudoexons, such as
378 that created by *MME* c.1188+428A>G, have also been described in *in vivo* preclinical
379 models[93,95–99]. As such, individuals with the *MME* c.1188+428A>G variant may represent a

form of CMT that is treatable through personalized ASO therapy and warrants further investigation.

Acknowledgements

This work was funded by the Medical Research Future Fund (MRFF) Genomics Health Futures Mission (APP2007681). JMP is supported by the Australian Government Research Training Program. IWD was supported by MRF2025138 & MRF2023126. Genomic analysis was supported by the Centre for Population Genomics (Garvan Institute of Medical Research and Murdoch Children's Research Institute) and was funded in part by a National Health and Medical Research Council investigator grant (2009982) and the Medical Research Future Fund (MRFF) Genomics Health Futures Mission (2008820).

391 **Figure Legends:**

392 **Figure 1: The *MME* c.1188+428A>G (NM_000902.5) variant segregates with recessive**
393 **CMT in two families**. A) Family 1 pedigree showing the associated genotypes for the *MME*
394 c.1188+428A>G (NM_000902.5) variant. Affected individuals in the fifth generation are
395 homozygous (G/G). Unaffected individuals in the fifth (V) and sixth (VI) generation are
396 heterozygous (A/G). Squares represent males and circles represent females, solid symbol
397 denotes affected individual. The double line in the fourth (IV) generation indicates a
398 consanguineous relationship. The *MME* c.1188+428 genotype is denoted beneath individuals
399 who underwent Sanger sequencing, with the pathogenic 'G' allele in red text. B) A pedigree
400 showing the associated genotypes for *MME* c.1188+428A>G and *MME* c.467del in the index
401 individual in Family 2. C-D) Haplotype phasing showed that the c.1188+428A>G (C) and
402 c.467del (D) variants were present on alternative haplotypes (light red and light blue), thus
403 inherited *in trans* in the proband of Family 2. Phased targeted ONT long-read sequencing
404 reads were visualized using the Integrative Genomics Viewer (IGV; v2.17.3).

405 **Figure 2. An exon-trapping assay was used to analyze splicing changes caused by the**
406 ***MME* c.1188+428A>G variant.** A) Schematic of the pSpliceExpress-MME_{WT} (wild-type)
407 and pSpliceExpress-$MME_{c.1188+428A>G}$ (variant) constructs. Both constructs consisted of an
408 RSV LTR promoter region (blue) controlling transcription of a minigene of *MME* exons 12
409 and 13 (grey) flanked by *Ins2* exon 2 and *Ins2* exon 3 (black). The constructs differed in the
410 presence of either an A (wild type: green text) or a G allele (mutant: red text) at *MME*
411 c.1188+428A>G. i) The wild type sequence was not predicted to contain any strong splice
412 sites when assessed using SpliceAI, with a score of 0.11 for the acceptor site (purple text) and
413 0.00 for the donor site (green text). ii) SpliceAI predicted that the *MME* c.1188+428A>G
414 variant (red arrow) would create a strong splice donor site [Score: 0.97 (Δ 0.97); red text],
415 which then strengthened the prediction of a splice acceptor site 83 bp upstream [Score 0.99

(Δ0.97); purple text]. The predicted 83 bp pseudoexon sequence is capitalized and boxed in red. B) The amplicon produced by the pSpliceExpress-*MME*$_{c.1188+428A>G}$ vector (464 bp) showed a visible increase in product size when compared to the amplicon produced by pSpliceExpress-*MME*$_{WT}$ (381 bp). The 158 bp RT-PCR product produced by both vectors indicated splicing and ligation of the flanking *Ins2* exon 2 and exon 3. Lanes: L: HyperLadder 100 bp (Bioline); WT: wild-type; NRTC: negative cDNA conversion control (no reverse transcriptase). NTC: negative PCR reaction control (no cDNA template). C) Sanger sequencing of the pSpliceExpress-*MME*$_{WT}$ RT-PCR product confirmed correct splicing between *MME* exon 12 and 13. D) Sanger sequencing of the pSpliceExpress-*MME*$_{c.1188+428A>G}$ RT-PCR product revealed the presence of a novel 83 bp pseudoexon (red) between *MME* exon 12 and 13. Abbreviations: RSV LTR: Rous Sarcoma Virus Long Terminal Repeat promoter; *Ins2*: rat preproinsulin 2 gene.

References

1. Skre H. Genetic and clinical aspects of Charcot-Marie-Tooth's disease. *Clin Genet*. 1974;6:98-118.

2. Szigeti K, Lupski JR. Charcot–Marie–Tooth disease. *European Journal of Human Genetics*. 2009;17(6):703-710. doi:10.1038/ejhg.2009.31

3. Senderek J, Lassuthova P, Kabzińska D, et al. The genetic landscape of axonal neuropathies in the middle-aged and elderly. *Neurology*. 2020;95(24). doi:10.1212/WNL.0000000000011132

4. Higuchi Y. Mutations in MME cause an autosomal-recessive Charcot-Marie-Tooth disease type 2. *Ann Neurol*. 2016;79:659-672.

5. Record CJ, Pipis M, Skorupinska M, et al. Whole genome sequencing increases the diagnostic rate in Charcot-Marie-Tooth disease. *Brain*. Published online March 14, 2024. doi:10.1093/brain/awae064

6. Jamiri Z, Khosravi R, Heidari MM, Kiani E, Gharechahi J. A nonsense mutation in <scp> *MME* </scp> gene associates with autosomal recessive late□onset <scp>Charcot–Marie–Tooth</scp> disease. *Mol Genet Genomic Med*. 2022;10(5). doi:10.1002/mgg3.1913

7. Taghizadeh S, Vazehan R, Beheshtian M, et al. Molecular Diagnosis of Hereditary Neuropathies by Whole Exome Sequencing and Expanding the Phenotype Spectrum. *Arch Iran Med*. 2020;23(7):426-433. doi:10.34172/AIM.2020.39

8. Ando M, Higuchi Y, Yuan J, et al. Comprehensive Genetic Analyses of Inherited Peripheral Neuropathies in Japan: Making Early Diagnosis Possible. *Biomedicines*. 2022;10(7):1546. doi:10.3390/biomedicines10071546

9. Megarbane A, Bizzari S, Deepthi A, et al. A 20-year Clinical and Genetic Neuromuscular Cohort Analysis in Lebanon: An International Effort. *J Neuromuscul Dis*. 2022;9(1):193-210. doi:10.3233/JND-210652

10. Høyer H, Hilmarsen HT, Sunder-Plassmann R, et al. A polymorphic AT-repeat causes frequent allele dropout for an *MME* mutational hotspot exon. *J Med Genet*. 2022;59(10):1024-1026. doi:10.1136/jmedgenet-2021-108281

11. Dupuis M, Raymackers JM, Ackermans N, Boulanger S, Verellen-Dumoulin C. Hereditary axonal neuropathy related to MME gene mutation in a family with fetomaternal alloimmune glomerulonephritis. *Acta Neurol Belg*. 2020;120(1):149-154. doi:10.1007/s13760-020-01275-9

12. Krämer HH, He L, Lu B, Birklein F, Sommer C. Increased pain and neurogenic inflammation in mice deficient of neutral endopeptidase. *Neurobiol Dis*. 2009;35(2):177-183. doi:10.1016/j.nbd.2008.11.002

13. Gemelli C, Geroldi A, Massucco S, et al. Genetic Workup for Charcot-Marie-Tooth Neuropathy: A Retrospective Single-Site Experience Covering 15 Years. *Life (Basel)*. 2022;12(3). doi:10.3390/life12030402

14. Candayan A, Parman Y, Battaloğlu E. Clinical and Genetic Survey for Charcot-Marie-Tooth Neuropathy Based on the Findings in Turkey, a Country with a High Rate of Consanguineous Marriages. *Balkan Med J*. 2022;39(1):3. doi:10.4274/BALKANMEDJ.GALENOS.2021.2021-11-13

15. Rudnik-Schöneborn S, Tölle D, Senderek J, et al. Diagnostic algorithms in Charcot-Marie-Tooth neuropathies: experiences from a German genetic laboratory on the basis of 1206 index patients. *Clin Genet*. 2016;89(1):34-43. doi:10.1111/cge.12594

16. Fridman V, Bundy B, Reilly MM, et al. CMT subtypes and disease burden in patients enrolled in the Inherited Neuropathies Consortium natural history study: a cross-sectional analysis. 2015;86(8):873-878. doi:10.1136/jnnp-2014-308826

17. Ma Y, Duan X, Liu X, Fan D. Clinical and mutational spectrum of paediatric Charcot-Marie-Tooth disease in a large cohort of Chinese patients. *Front Genet*. 2023;14. doi:10.3389/fgene.2023.1188361

18. Lord J, Baralle D. Splicing in the Diagnosis of Rare Disease: Advances and Challenges. *Front Genet*. 2021;12:689892. doi:10.3389/fgene.2021.689892

19. Wang R, Helbig I, Edmondson AC, Lin L, Xing Y. Splicing defects in rare diseases: transcriptomics and machine learning strategies towards genetic diagnosis. *Brief Bioinform*. 2023;24(5). doi:10.1093/bib/bbad284

20. Anna A, Monika G. *Splicing Mutations in Human Genetic Disorders: Examples, Detection, and Confirmation*. Vol 59. Springer Verlag; 2018:253-268. doi:10.1007/s13353-018-0444-7

21. Corrado L, Magri S, Bagarotti A, et al. A novel synonymous mutation in the MPZ gene causing an aberrant splicing pattern and Charcot-Marie-Tooth disease type 1b. *Neuromuscular Disorders*. 2016;26(8):516-520. doi:10.1016/j.nmd.2016.05.011

22. Boaretto F, Vettori A, Casarin A, et al. Severe CMT type 2 with fatal encephalopathy associated with a novel MFN2 splicing mutation. *Neurology*. 2010;74(23). doi:10.1212/WNL.0b013e3181e240f9

23. Engeholm M, Sekler J, Schöndorf DC, et al. A novel mutation in LRSAM1 causes axonal Charcot-Marie-Tooth disease with dominant inheritance. *BMC Neurol*. 2014;14(1):118. doi:10.1186/1471-2377-14-118

24. Cassini TA, Duncan L, Rives LC, et al. Whole genome sequencing reveals novel *IGHMBP2* variant leading to unique cryptic splice□site and Charcot□Marie□Tooth phenotype with early onset symptoms. *Mol Genet Genomic Med*. 2019;7(6):e00676. doi:10.1002/mgg3.676

25. Echaniz□Laguna A, Latour P, Echaniz-Laguna A, Latour P, Echaniz□Laguna A, Latour P. A cryptic splicing mutation in the INF2 gene causing Charcot-Marie-Tooth

disease with minimal glomerular dysfunction. *Journal of the Peripheral Nervous System*. 2019;24(1):120-124. doi:10.1111/jns.12308

26. Ylikallio E, Woldegebriel R, Tumiati M, et al. MCM3AP in recessive Charcot-Marie-Tooth neuropathy and mild intellectual disability. *Brain*. 2017;140(8):2093-2103. doi:10.1093/brain/awx138

27. Numakura C, Lin C, Ikegami T, Guldberg P, Hayasaka K. Molecular analysis in Japanese patients with Charcot-Marie-Tooth disease: DGGE analysis for PMP22, MPZ, and Cx32/GJB1 mutations. *Hum Mutat*. 2002;20(5):392-398. doi:10.1002/humu.10134

28. Flusser H, Halperin D, Kadir R, Shorer Z, Shelef I, Birk OS. Novel SBF1 splice-site null mutation broadens the clinical spectrum of Charcot-Marie-Tooth type 4B3 disease. *Clin Genet*. 2018;94(5):473-479. doi:10.1111/cge.13419

29. Hayashi M, Abe A, Murakami T, et al. Molecular analysis of the genes causing recessive demyelinating Charcot-Marie-Tooth disease in Japan. *J Hum Genet*. 2013;58(5):273-278. doi:10.1038/jhg.2013.15

30. DiVincenzo C, Elzinga CD, Medeiros AC, et al. The allelic spectrum of Charcot-Marie-Tooth disease in over 17,000 individuals with neuropathy. *Mol Genet Genomic Med*. 2014;2(6):522-529. doi:10.1002/mgg3.106

31. Martikainen MH, Kytövuori L, Majamaa K. Novel mitofusin 2 splice-site mutation causes Charcot–Marie–Tooth disease type 2 with prominent sensory dysfunction. *Neuromuscular Disorders*. 2014;24(4):360-364. doi:10.1016/J.NMD.2014.01.007

32. Piscosquito G, Saveri P, Magri S, et al. Screening for SH3TC2 gene mutations in a series of demyelinating recessive Charcot-Marie-Tooth disease (CMT4). *J Peripher Nerv Syst*. 2016;21(3):142-149. doi:10.1111/jns.12175

33. Benedetti S, Previtali SC, Coviello S, et al. Analyzing histopathological features of rare Charcot-Marie-Tooth neuropathies to unravel their pathogenesis. *Arch Neurol*. 2010;67(12):1498-1505. doi:10.1001/archneurol.2010.303

34. Li MY, Yin M, Yang L, et al. A novel splicing mutation in 5'UTR of GJB1 causes X-linked Charcot—Marie–tooth disease. *Mol Genet Genomic Med*. 2023;11(3):e2108. doi:10.1002/MGG3.2108

35. Boso F, Taioli F, Cabrini I, Cavallaro T, Fabrizi GM. Aberrant Splicing in GJB1 and the Relevance of 5′ UTR in CMTX1 Pathogenesis. *Brain Sci*. 2020;11(1):24. doi:10.3390/brainsci11010024

36. Tomaselli PJPPJ, Rossor AM, Horga A, et al. Mutations in noncoding regions in GJB1 are a major cause of X-linked CMT. *Neurology*. 2017;88(15):1445-1453. doi:10.1212/WNL.0000000000003819

37. Pravinbabu P, Holla V V, Phulpagar P, et al. A splice altering variant in NDRG1 gene causes Charcot-Marie-Tooth disease, type 4D. *Neurol Sci*. 2022;43(7):4463-4472. doi:10.1007/s10072-022-05893-4

545 38. Shchagina O, Orlova M, Murtazina A, Filatova A, Skoblov M, Dadali E. Evaluation of
546 Pathogenicity and Causativity of Variants in the MPZ and SH3TC2 Genes in a Family
547 Case of Hereditary Peripheral Neuropathy. *Int J Mol Sci*. 2023;24(12).
548 doi:10.3390/ijms24129786

549 39. Taioli F, Cabrini I, Cavallaro T, Simonati A, Testi S, Fabrizi GM. Déjerine-Sottas
550 syndrome with a silent nucleotide change of myelin protein zero gene. *Journal of the*
551 *Peripheral Nervous System*. 2011;16(1):59-64. doi:10.1111/j.1529-8027.2011.00319.x

552 40. Sabet A, Li J, Ghandour K, et al. Skin biopsies demonstrate MPZ splicing
553 abnormalities in Charcot-Marie-Tooth neuropathy 1B. *Neurology*. 2006;67(7):1141-
554 1146. doi:10.1212/01.wnl.0000238499.37764.b1

555 41. Lupo V. Characterising the phenotype and mode of inheritance of patients with
556 inherited peripheral neuropathies carrying MME mutations. *J Med Genet*.
557 2018;55:814-823.

558 42. Masingue M, Perrot J, Carlier RY, Piguet-Lacroix G, Latour P, Stojkovic T. WES
559 homozygosity mapping in a recessive form of Charcot-Marie-Tooth neuropathy
560 reveals intronic GDAP1 variant leading to a premature stop codon. *Neurogenetics*.
561 2018;19(2):67-76. doi:10.1007/s10048-018-0539-7

562 43. Duyk GM, Kim SW, Myers RM, Cox DR. Exon trapping: a genetic screen to identify
563 candidate transcribed sequences in cloned mammalian genomic DNA. *Proceedings of*
564 *the National Academy of Sciences*. 1990;87(22):8995-8999.
565 doi:10.1073/pnas.87.22.8995

566 44. Micale L, Morlino S, Schirizzi A, et al. Exon-Trapping Assay Improves Clinical
567 Interpretation of COL11A1 and COL11A2 Intronic Variants in Stickler Syndrome
568 Type 2 and Otospondylomegaepiphyseal Dysplasia. *Genes (Basel)*. 2020;11(12):1513.
569 doi:10.3390/genes11121513

570 45. Grosz BR, Tisch S, Tchan MC, et al. A novel synonymous KMT2B variant in a patient
571 with dystonia causes aberrant splicing. *Mol Genet Genomic Med*. 2022;10(5).
572 doi:10.1002/MGG3.1923

573 46. Mutai H, Wasano K, Momozawa Y, et al. Variants encoding a restricted carboxy-
574 terminal domain of SLC12A2 cause hereditary hearing loss in humans. *PLoS Genet*.
575 2020;16(4). doi:10.1371/journal.pgen.1008643

576 47. Knapp KM, Sullivan R, Murray J, et al. Linked-read genome sequencing identifies
577 biallelic pathogenic variants in DONSON as a novel cause of Meier-Gorlin syndrome.
578 *J Med Genet*. 2020;57(3):195-202. doi:10.1136/jmedgenet-2019-106396

579 48. Starokadomskyy P, Gemelli T, Rios JJ, et al. DNA polymerase-α regulates the
580 activation of type i interferons through cytosolic RNA:DNA synthesis. *Nat Immunol*.
581 2016;17(5):495-504. doi:10.1038/ni.3409

582 49. Varga L, Danis D, Skopkova M, et al. Novel EYA4 variant in Slovak family with late
583 onset autosomal dominant hearing loss: A case report. *BMC Med Genet*. 2019;20(1).
584 doi:10.1186/s12881-019-0806-y

50. Legendre M, Rodriguez-Ballesteros M, Rossi M, et al. CHARGE syndrome: A recurrent hotspot of mutations in CHD7 IVS25 analyzed by bioinformatic tools and minigene assays /631/208 /692/308 brief-communication. *European Journal of Human Genetics*. 2018;26(2):287-292. doi:10.1038/s41431-017-0007-0

51. Abdulhay NJ, Fiorini C, Verboon JM, et al. Impaired human hematopoiesis due to a cryptic intronic GATA1 splicing mutation. *Journal of Experimental Medicine*. 2019;216(5):1050-1060. doi:10.1084/jem.20181625

52. Kishore S, Khanna A, Stamm S. Rapid generation of splicing reporters with pSpliceExpress. *Gene*. 2008;427(1-2):104-110. doi:10.1016/j.gene.2008.09.021

53. Pedersen BS, Bhetariya PJ, Brown J, et al. Somalier: rapid relatedness estimation for cancer and germline studies using efficient genome sketches. *Genome Med*. 2020;12(1):62. doi:10.1186/s13073-020-00761-2

54. Pais LS, Snow H, Weisburd B, et al. seqr: A web-based analysis and collaboration tool for rare disease genomics. *Hum Mutat*. 2022;43(6):698-707. doi:10.1002/HUMU.24366

55. Stark Z, Foulger RE, Williams E, et al. Scaling national and international improvement in virtual gene panel curation via a collaborative approach to discordance resolution. *Am J Hum Genet*. 2021;108(9):1551-1557. doi:10.1016/j.ajhg.2021.06.020

56. Jaganathan K, Kyriazopoulou Panagiotopoulou S, McRae JF, et al. Predicting Splicing from Primary Sequence with Deep Learning. *Cell*. 2019;176(3):535-548.e24. doi:10.1016/j.cell.2018.12.015

57. Payne A, Holmes N, Clarke T, Munro R, Debebe BJ, Loose M. Readfish enables targeted nanopore sequencing of gigabase-sized genomes. *Nat Biotechnol*. 2021;39(4):442-450. doi:10.1038/s41587-020-00746-x

58. Stevanovski I, Chintalaphani SR, Gamaarachchi H, et al. Comprehensive genetic diagnosis of tandem repeat expansion disorders with programmable targeted nanopore sequencing. *Sci Adv*. 2022;8(9). doi:10.1126/SCIADV.ABM5386

59. Gamaarachchi H, Samarakoon H, Jenner SP, et al. Fast nanopore sequencing data analysis with SLOW5. *Nat Biotechnol*. 2022;40(7):1026-1029. doi:10.1038/s41587-021-01147-4

60. Samarakoon H, Ferguson JM, Jenner SP, et al. Flexible and efficient handling of nanopore sequencing signal data with slow5tools. *Genome Biol*. 2023;24(1):69. doi:10.1186/s13059-023-02910-3

61. Li H. Minimap2: pairwise alignment for nucleotide sequences. *Bioinformatics*. 2018;34(18):3094-3100. doi:10.1093/bioinformatics/bty191

62. Zheng Z, Li S, Su J, Leung AWS, Lam TW, Luo R. Symphonizing pileup and full-alignment for deep learning-based long-read variant calling. *Nat Comput Sci*. 2022;2(12):797-803. doi:10.1038/s43588-022-00387-x

63. Martin M, Patterson M, Garg S, et al. WhatsHap: fast and accurate read-based phasing. Published online 2016. doi:10.1101/085050

64. Robinson JT, Thorvaldsdóttir H, Winckler W, et al. Integrative Genomics Viewer. *Nat Biotechnol*. 2011;29(1):24. doi:10.1038/NBT.1754

65. Zeng Z, Bromberg Y. Predicting Functional Effects of Synonymous Variants: A Systematic Review and Perspectives. *Front Genet*. 2019;0:914. doi:10.3389/FGENE.2019.00914

66. Kishore Jaganathan A, Kyriazopoulou Panagiotopoulou S, McRae JF, et al. Predicting Splicing from Primary Sequence with Deep Learning In Brief A deep neural network precisely models mRNA splicing from a genomic sequence and accurately predicts noncoding cryptic splice mutations in patients with rare genetic diseases. Predicting Splicing from Primary Sequence with Deep Learning. *Cell*. 2018;176:535-548. doi:10.1016/j.cell.2018.12.015

67. Sherry ST, Ward MH, Kholodov M, et al. dbSNP: the NCBI database of genetic variation. *Nucleic Acids Res*. 2001;29(1):308-311. Accessed March 5, 2019. http://www.ncbi.nlm.nih.gov/pubmed/11125122

68. Chen S, Francioli LC, Goodrich JK, et al. A genomic mutational constraint map using variation in 76,156 human genomes. *Nature*. 2024;625(7993):92-100. doi:10.1038/s41586-023-06045-0

69. All of Us Research Program Investigators, Denny JC, Rutter JL, et al. The "All of Us" Research Program. *N Engl J Med*. 2019;381(7):668-676. doi:10.1056/NEJMsr1809937

70. Taliun D, Harris DN, Kessler MD, et al. Sequencing of 53,831 diverse genomes from the NHLBI TOPMed Program. *Nature*. 2021;590(7845):290-299. doi:10.1038/s41586-021-03205-y

71. Kent WJ. <tt>BLAT</tt> —The <tt>BLAST</tt> -Like Alignment Tool. *Genome Res*. 2002;12(4):656-664. doi:10.1101/gr.229202

72. Castle JC. SNPs occur in regions with less genomic sequence conservation. *PLoS One*. 2011;6(6):e20660. doi:10.1371/journal.pone.0020660

73. Boisson M, Arrondel C, Cagnard N, et al. A wave of deep intronic mutations in X-linked Alport syndrome. *Kidney Int*. 2023;104(2):367-377. doi:10.1016/j.kint.2023.05.006

74. Qian X, Wang J, Wang M, et al. Identification of Deep-Intronic Splice Mutations in a Large Cohort of Patients With Inherited Retinal Diseases. *Front Genet*. 2021;12:647400. doi:10.3389/fgene.2021.647400

75. Di Scipio M, Tavares E, Deshmukh S, et al. Phenotype Driven Analysis of Whole Genome Sequencing Identifies Deep Intronic Variants that Cause Retinal Dystrophies by Aberrant Exonization. *Invest Ophthalmol Vis Sci*. 2020;61(10):36. doi:10.1167/iovs.61.10.36

76. Xie Z, Sun C, Liu Y, et al. Practical approach to the genetic diagnosis of unsolved dystrophinopathies: a stepwise strategy in the genomic era. *J Med Genet*. 2021;58(11):743-751. doi:10.1136/jmedgenet-2020-107113

77. Zaum AK, Stüve B, Gehrig A, et al. Deep intronic variants introduce DMD pseudoexon in patient with muscular dystrophy. *Neuromuscul Disord*. 2017;27(7):631-634. doi:10.1016/j.nmd.2017.04.003

78. Anna A, Monika G. Splicing mutations in human genetic disorders: examples, detection, and confirmation. *J Appl Genet*. 2018;59(3):253-268. doi:10.1007/s13353-018-0444-7

79. Richards S, Aziz N, Bale S, et al. Standards and guidelines for the interpretation of sequence variants: A joint consensus recommendation of the American College of Medical Genetics and Genomics and the Association for Molecular Pathology. *Genetics in Medicine*. 2015;17(5):405-424. doi:10.1038/gim.2015.30

80. Depondt C, Donatello S, Rai M, et al. MME mutation in dominant spinocerebellar ataxia with neuropathy (SCA43). *Neurol Genet*. 2016;2(5):e94. doi:10.1212/NXG.0000000000000094

81. Kim J, Woo S, de Gusmao CM, et al. A framework for individualized splice-switching oligonucleotide therapy. *Nature*. 2023;619(7971):828-836. doi:10.1038/s41586-023-06277-0

82. Chen S, Heendeniya SN, Le BT, et al. Splice-Modulating Antisense Oligonucleotides as Therapeutics for Inherited Metabolic Diseases. *BioDrugs*. 2024;38(2):177-203. doi:10.1007/s40259-024-00644-7

83. Santos JI, Gonçalves M, Matos L, et al. Splicing Modulation as a Promising Therapeutic Strategy for Lysosomal Storage Disorders: The Mucopolysaccharidoses Example. *Life*. 2022;12(5):608. doi:10.3390/life12050608

84. Mendell JR, Rodino-Klapac LR, Sahenk Z, et al. Eteplirsen for the treatment of Duchenne muscular dystrophy. *Ann Neurol*. 2013;74(5):637-647. doi:10.1002/ana.23982

85. Frank DE, Schnell FJ, Akana C, et al. Increased dystrophin production with golodirsen in patients with Duchenne muscular dystrophy. *Neurology*. 2020;94(21):e2270-e2282. doi:10.1212/WNL.0000000000009233

86. Heo YA. Golodirsen: First Approval. *Drugs*. 2020;80(3):329-333. doi:10.1007/s40265-020-01267-2

87. Clemens PR, Rao VK, Connolly AM, et al. Safety, Tolerability, and Efficacy of Viltolarsen in Boys With Duchenne Muscular Dystrophy Amenable to Exon 53 Skipping: A Phase 2 Randomized Clinical Trial. *JAMA Neurol*. 2020;77(8):982-991. doi:10.1001/jamaneurol.2020.1264

88. Shirley M. Casimersen: First Approval. *Drugs*. 2021;81(7):875-879. doi:10.1007/s40265-021-01512-2

89. Wurster CD, Winter B, Wollinsky K, et al. Intrathecal administration of nusinersen in adolescent and adult SMA type 2 and 3 patients. *J Neurol*. 2019;266(1):183-194. doi:10.1007/s00415-018-9124-0

90. Osredkar D, Jílková M, Butenko T, et al. Children and young adults with spinal muscular atrophy treated with nusinersen. *Eur J Paediatr Neurol*. 2021;30:1-8. doi:10.1016/j.ejpn.2020.11.004

91. Mercuri E, Darras BT, Chiriboga CA, et al. Nusinersen versus Sham Control in Later-Onset Spinal Muscular Atrophy. *N Engl J Med*. 2018;378(7):625-635. doi:10.1056/NEJMoa1710504

92. Bianchi L, Sframeli M, Vantaggiato L, et al. Nusinersen Modulates Proteomics Profiles of Cerebrospinal Fluid in Spinal Muscular Atrophy Type 1 Patients. *Int J Mol Sci*. 2021;22(9). doi:10.3390/ijms22094329

93. Kim J, Woo S, de Gusmao CM, et al. A framework for individualized splice-switching oligonucleotide therapy. *Nature*. 2023;619(7971):828-836. doi:10.1038/s41586-023-06277-0

94. Kim J, Hu C, Moufawad El Achkar C, et al. Patient-Customized Oligonucleotide Therapy for a Rare Genetic Disease. *N Engl J Med*. 2019;381(17):1644-1652. doi:10.1056/NEJMoa1813279

95. Yamada M, Maeta K, Suzuki H, et al. Successful skipping of abnormal pseudoexon by antisense oligonucleotides in vitro for a patient with beta-propeller protein-associated neurodegeneration. *Sci Rep*. 2024;14(1):6506. doi:10.1038/s41598-024-56704-z

96. Aguti S, Bolduc V, Ala P, et al. Exon-Skipping Oligonucleotides Restore Functional Collagen VI by Correcting a Common COL6A1 Mutation in Ullrich CMD. *Mol Ther Nucleic Acids*. 2020;21:205-216. doi:10.1016/J.OMTN.2020.05.029

97. Kim J, Hu C, Moufawad El Achkar C, et al. Patient-Customized Oligonucleotide Therapy for a Rare Genetic Disease. *N Engl J Med*. 2019;381(17):1644-1652. doi:10.1056/NEJMOA1813279

98. Dominov JA, Uyan Ö, McKenna□Yasek D, et al. Correction of pseudoexon splicing caused by a novel intronic dysferlin mutation. *Ann Clin Transl Neurol*. 2019;6(4):642-654. doi:10.1002/acn3.738

99. Martínez-Pizarro A, Leal F, Holm LL, et al. Antisense Oligonucleotide Rescue of Deep-Intronic Variants Activating Pseudoexons in the 6-Pyruvoyl-Tetrahydropterin Synthase Gene. *Nucleic Acid Ther*. 2022;32(5):378-390. doi:10.1089/nat.2021.0066

Table 1. Phenotypic characterization of individuals with recessive CMT *MME* variants reported in this manuscript. Abbreviations- AFO: Ankle foot orthoses; CMTNS: Charcot-Marie-Tooth Neuropathy Score; UL/LL: Upper Limb/Lower Limb

Family #	**Family 1**				**Family 2**
Individual	**V:1**	**V:3**	**V:4**	**V:6**	**II:1**
Sex	M	F	M	M	F
Onset	Fourth decade	Childhood	Childhood	Childhood	Early-adult
Age at evaluation (years)	60-65	65-70	65-70	65-70	50-55
Presenting symptom	Gait unsteadiness	Difficulty running	Difficulty sitting on crossed legs during childhood	Difficulty running, multiple ankle sprains	Bilateral leg weakness and sensory disturbance
Atrophy UL/LL	Yes/yes	Yes/yes	Yes/yes	Yes/yes	No/Yes (left calf only)
Foot deformity	None	Pes cavus/hammer toes	-	Pes cavus	Pes cavus
Tone UL/LL	Normal/reduced	Normal/normal	Normal, increased		Normal/normal
Shoulder abduction	5	5	3	5	4
Elbow flexion	4	5	3	4	5
Elbow extension	4	5	3	4	5

Finger abduction	2	4	3	1	4
Hip flexion	4	3	3	3	4
Knee extension	4	3	3	4	4
Knee flexion	4	3	3	4	4
Ankle dorsiflexion	0	0	3	1	3
Ankle plantarflexion	0	0	3	0	4
Deep tendon reflexes UL/LL	Absent/absent	Absent ankle	Hyperreflexia knee, absent ankle	Absent/absent	Normal/ reduced ankle reflexes
Plantars	Absent	-	Absent	Flexor	Flexor
Proprioception UL/LL	Normal/reduced to the MTP	-	-	Normal/reduced to the ankle	Normal/reduced to ankle
Vibration UL/LL	Normal/reduced to ankle	Absent in toes	-	Reduced to wrist/reduced to knees	Reduced to mid-shin
Pinprick UL/LL	Normal/reduced to ankle	Normal/reduced to the mid shin	Reduced to elbows/reduced to knees	Reduced to PIP joint/reduced to knees	Reduced to mid-shin Reduced dorsum hand
Temperature sensation UL/LL	Normal/reduced to ankle	-	-	Reduced to wrist/reduced to above	Reduced to mid-shin

				knee	
Other symptoms/signs	Cough	GORD and cough	Corticospinal tract signs	Nil	Fatty infiltration on left gastrocnemius
Gait	High steppage/ataxic	High steppage/ataxic	Steppage gait	High steppage/ataxic	High steppage
Romberg's sign	Positive	Positive		Positive	Mild sway
Mobility aids	AFO, walking stick and mobility scooter	AFO, walker	AFO, walker, mobility scooter	Wheelchair	AFO, elbow crutch
CMTNS (version 2)	31	-	28/36	36	15

Table 2. Nerve conduction study (NCS) findings of individuals with recessive CMT *MME* variants reported in this manuscript. Abbreviations: APB: abductor pollicis brevis; ADM: abductor digiti minimi; EDB: extensor hallucis brevis; FHB: flexor hallus brevis; CMAP: compound motor action potential; CV: conduction velocity; NR: no response; SNAP: sensory nerve action potential; R: right, L:left.

Family #	**Family 1**		**Family 2**
Individual	**V:1**	**V:6**	**II:1**
Age at NCS (years)	60-65	65-70	55-60
Median nerve (digit II) [orthodromic(R)]			
SNAP (uV)	NR	NR	6.6
CV (m/s)	NR	NR	50
Ulnar nerve (digit V) [orthodromic(R)]			
SNAP (uV)	NR	1	4.9
CV (m/s)	NR	40.2	51
Sural nerve [orthodromic(R)]			
SNAP (uV)	NR	NR	NR
CV (m/s)	NR	NR	NR
Sural nerve [orthodromic(L)]			

SNAP (uV)	NR	NR	NR
CV (m/s)	NR	NR	NR
Median nerve (APB) (R)			
CMAP (mV)	NR	NR	4.8
CV (m/s)	NR	NR	41
Ulnar nerve (ADM) (R)			
CMAP (mV)	2	0.6	6.6
CV (m/s)	44.4	44.7	52 (wrist-below elbow) 57 (wrist-above elbow)
Peroneal nerve (EDB) (R)			
CMAP (mV)	NR	NR	NR
CV (m/s)	NR	NR	NR
Tibial nerve (FHB) (L)			
CMAP (mV)	NR	NR	NR
CV (m/s)	NR	NR	NR
Needle EMG	Absent voluntary units in the right tibilias anterior and medial gastrocnemius muscles, as well as denervation-reinnervation changes in	Absent recruitment of motor units in the right tibialis anterior, medical gastrocnemius, first dorsal interosseous and vastus lateralis	Reduced recruitment of motor units in the right tibialis interior and right vastus medialis muscles. Discrete recruitment of muscle fibres in the

	the right vastus lateralis muscle.	muscles. Denervation-reinnervation changes were evident in the right deltoid, biceps brachii and triceps brachii muscles.	right gastrocnemius muscle.

a

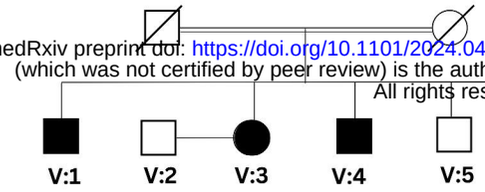

MME c.1188+428A>G

b

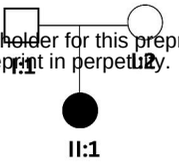

A / G *MME* c.1188+428A>G

- / C *MME* c.467del

c

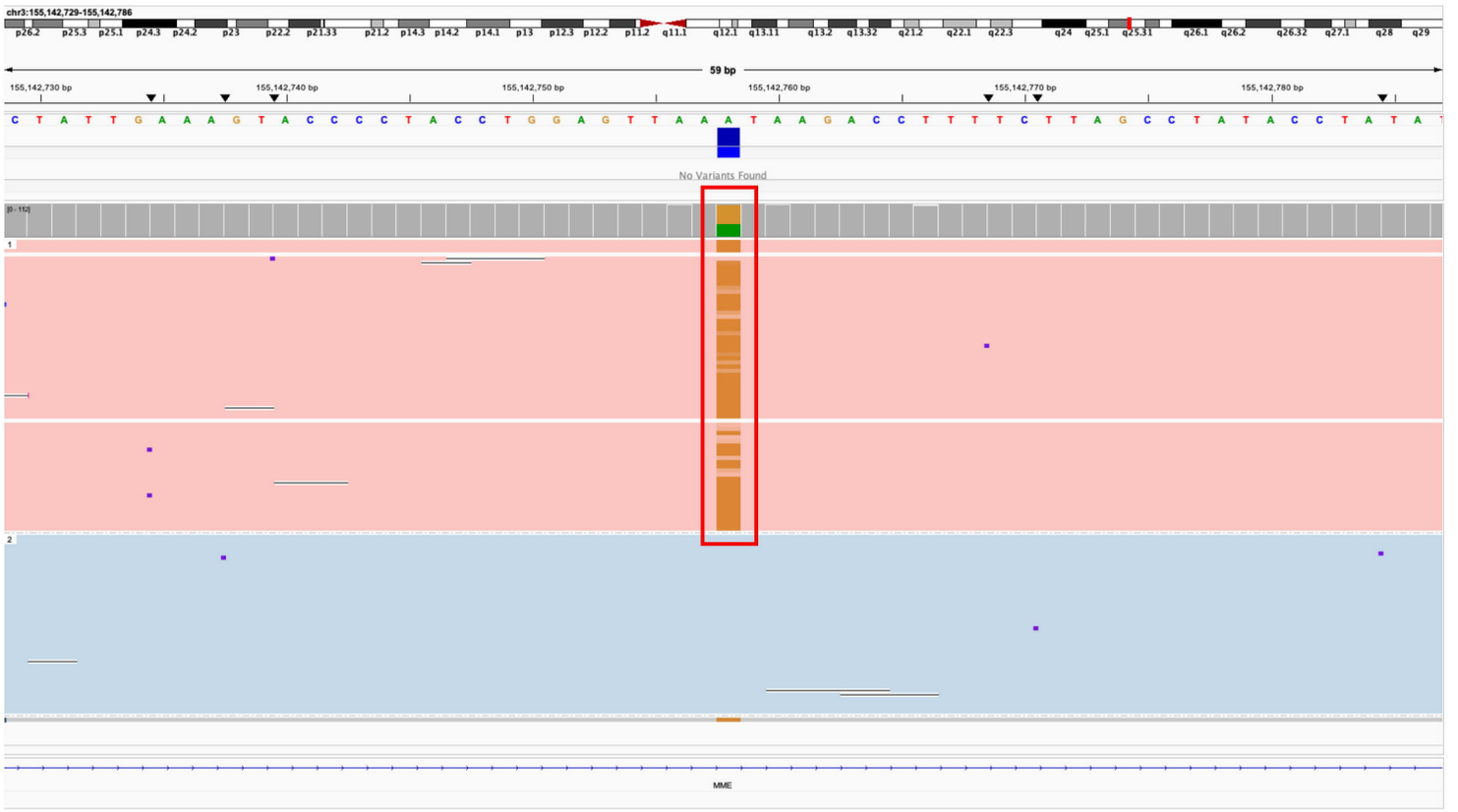

d

a

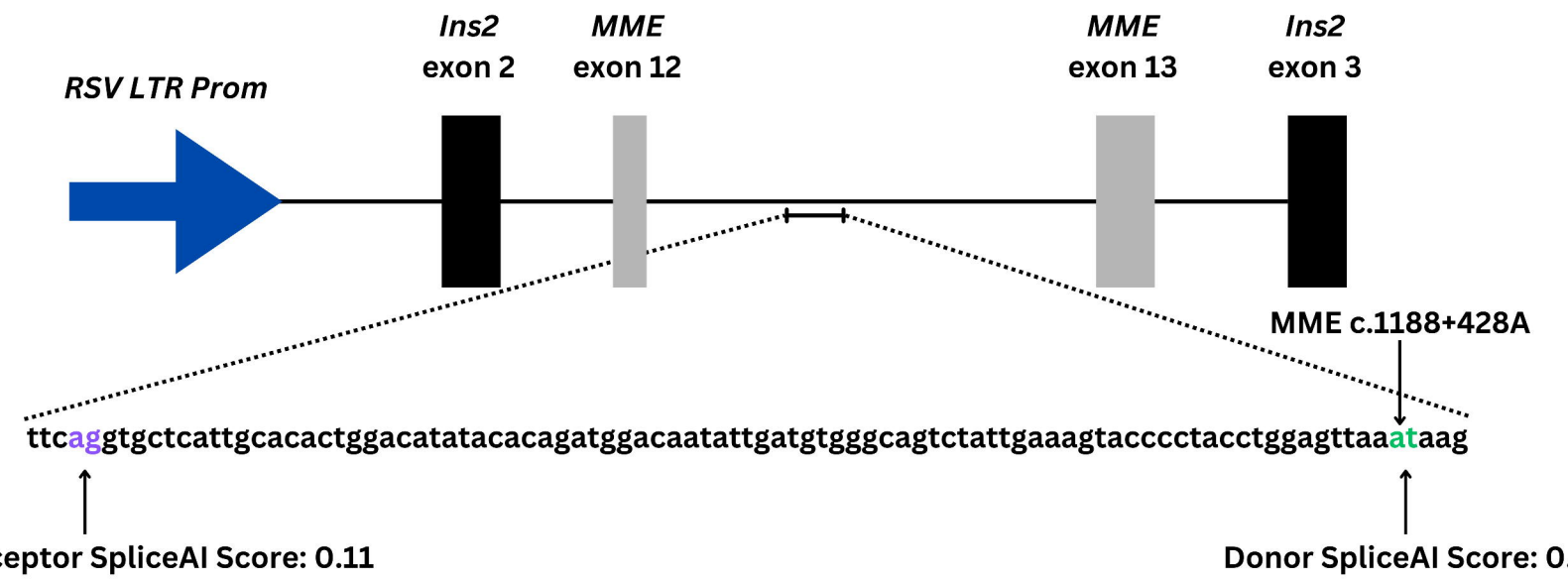

i.

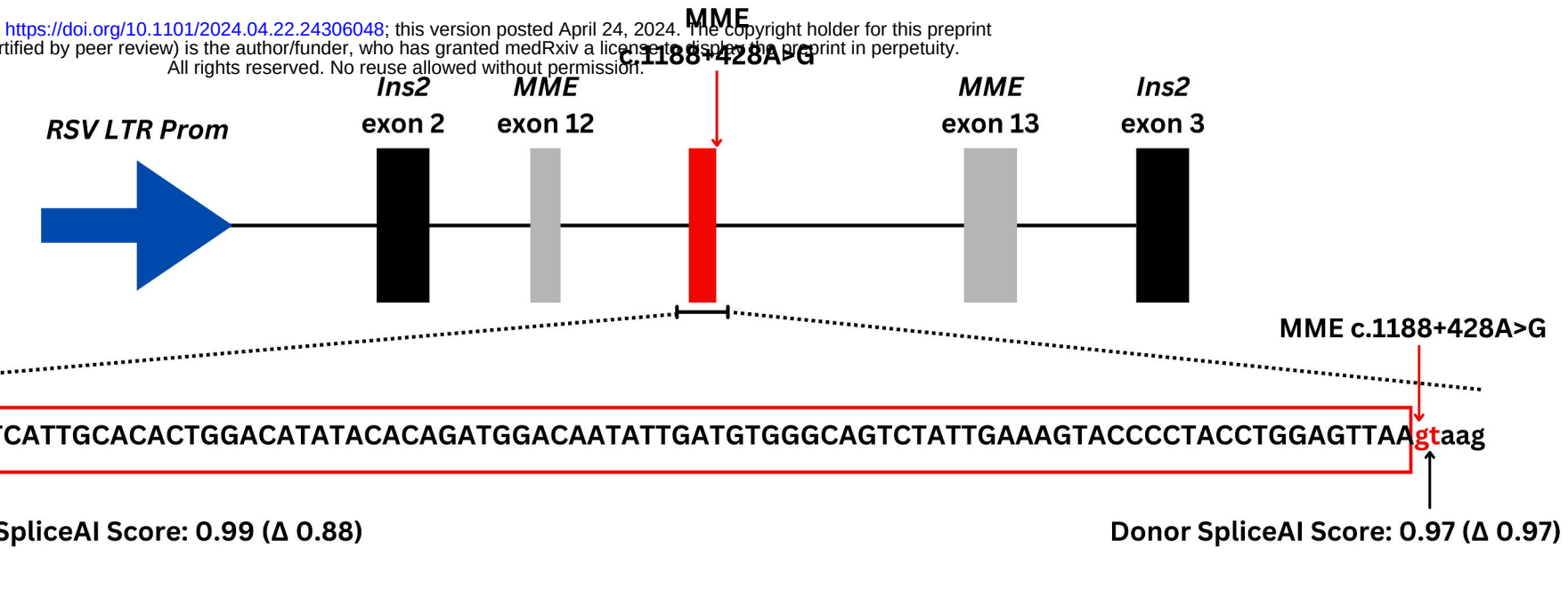

ii.

b

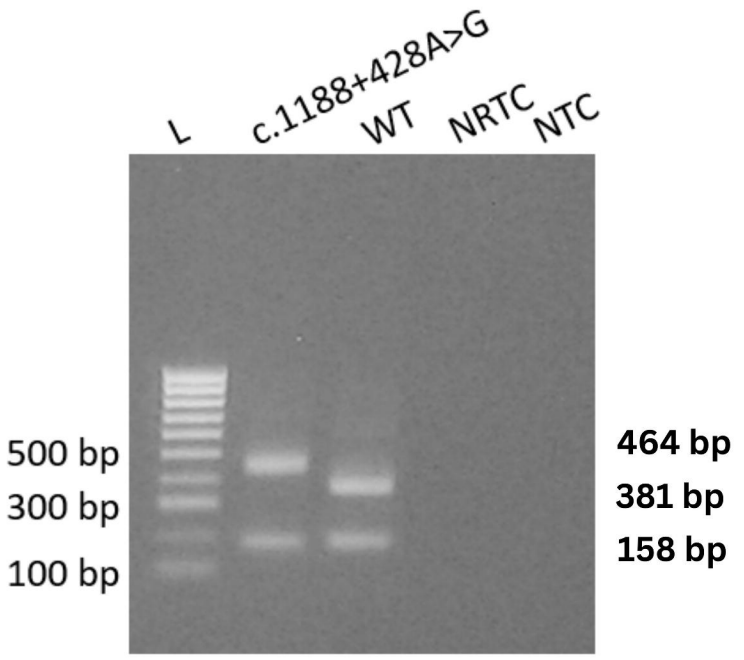

c

d